# Infrared spectroscopy of narrow gap donor-acceptor polymer-based ambipolar transistors

O. Khatib,[1,*] J. D. Yuen,[2] J. Wilson,[1] R. Kumar,[2] M. Di Ventra,[1] A. J. Heeger,[2] and D. N. Basov[1]

[1]*Department of Physics, University of California San Diego, La Jolla, California 92093, USA*
[2]*Center for Polymers and Organic Solids, University of California Santa Barbara, Santa Barbara, California 93106, USA*
(Received 12 July 2012; published 7 November 2012)

Donor-acceptor (D-A) copolymers have recently emerged as versatile materials for use in a large variety of device applications. Specifically, these systems possess extremely narrow band gaps, enabling ambipolar charge transport when integrated in solution-processed organic field-effect transistors (OFETs). However, the fundamentals of electronic transport in this class of materials remain unexplored. We present a systematic investigation of ambipolar charge injection in narrow-gap D-A conjugated polymers polybenzobisthiadiazole-dithienopyrrole (PBBTPD) and polybenzobisthiadiazole-dithienocyclopentane (PBBTCD) using infrared (IR) spectroscopy. We observe a significant modification of the absorption edge in both PBBTPD- and PBBTCD-based OFETs under the applied electric field. The absorption edge reveals hardening under electron injection and softening under hole injection. Additionally, we register localized vibrational resonances associated with injected charges. Our findings indicate a significant self-doping of holes that is modified by charge injection. Observations of both electron and hole transport with relatively high carrier mobility strongly suggest an inhomogeneous, phase-separated conducting polymer.

## I. INTRODUCTION

Organic semiconductors have emerged as attractive materials for use in a variety of large-area, low-cost electronic applications.[1,2] Recently, organic field-effect transistors (OFETs) based on solution-processed conjugated polymers have attained carrier mobilities exceeding 1 cm$^2$ V$^{-1}$ s$^{-1}$ for unipolar *p*-type[3] and *n*-type devices.[4] There is considerable interest in ambipolar polymers for use in organic complementary logic electronics similar to standard silicon CMOS technology.[5] One very efficient way to achieve intrinsic ambipolarity in conjugated polymers is through the use of donor-acceptor (DA) structures.[6–8] With appropriate choices for donor and acceptor moieties, electron and hole injection barriers can be minimized by effectively tuning the highest-occupied (HOMO) and lowest-unoccupied (LUMO) molecular orbitals of the DA polymer.[9–11] This inherent tunability has enabled fabrication of polymers with extremely narrow energy band gaps, highlighting DA systems as useful materials for photovoltaic and light-emitting devices.[12] When incorporated in ambipolar OFETs, DA polymers allow for a detailed investigation into mechanisms of electrostatic injection of both electrons and holes into a polymer host. Very recently, a new class of DA polymers based on electron acceptor benzobisthiadiazole (BBT) have demonstrated an ambipolar OFET operation with reasonably high carrier mobilities[13] between $10^{-2}$ and $10^{-1}$ cm$^2$ V$^{-1}$ s$^{-1}$. Additionally, these systems possess extremely narrow band gaps below 1 eV, as well as many other unusual optical, electrochemical, and transistor properties.[8,13–15] Polymers with such small energy gaps alleviate large injection barrier issues that prevent a thorough study of both electron and hole doping in systems employing commonly used gold electrodes.

We present a systematic investigation of ambipolar charge injection in OFETs based on narrow-gap DA conjugated polymers polybenzobisthiadiazole-dithienopyrrole (PBBTPD) and polybenzobisthiadiazole-dithienocyclopentane (PBBTCD) using infrared (IR) spectroscopy. IR methods have the advantage of directly probing the electronic excitations associated with charge injection.[16–19] A detailed characterization of the ungated polymer absorption edge in the mid-IR is carried out using spectroscopic ellipsometry. We then observed a significant modification of the absorption edge in both PBBTPD- and PBBTCD-based OFETs under the applied electric field. The absorption edge reveals hardening under electron injection and softening under hole injection. In addition to this field-induced behavior near the polymer band edge, we find evidence of localized charge carriers in the form of sharp vibrational resonances at lower energies. We critically assess the possible role of several physical mechanisms that can be responsible for these voltage-dependent features in the IR transmission data, including absorption due to charged molecular species (i.e., polarons).

## II. EXPERIMENT

A detailed description of polymer synthesis and sample preparation for poly[(4,7-bis(3-hexylthien-2-yl)-2λ4δ2-benzo[1,2-c;4,5-c′]bis[1,2,5]thiadiazole)-alt-(N-(3,4,5-tris(dodecyloxy) phenyl)-dithieno[3,2-b:2′,3′-d]pyrrole)] (PBBTPD) and poly[(4,7-bis(3-hexylthien-2-yl)-2λ4δ2-benzo[1,2-c;4,5-c′]bis[1,2,5]thiadiazole)-alt-(3,3-bis(2-ethyl hexyl) 4H-cyclopenta[2,1-b:3,4-b′]dithiophene)] (PBBTCD) can be found in Ref. 13.

Partially transparent 20–30 Ω cm *n*-doped Si wafers served as the backgate in devices employing two types of dielectrics: SiO$_2$ ($\epsilon = 3.9$) and Ta$_2$O$_5$ ($\epsilon = 24$). Electrodes were patterned using standard photolithography and were formed with *e*-beam evaporation of 3 nm of nickel followed by 47 nm of gold. Thin 25 nm polymer films were spin-coated onto substrate surfaces treated with decyltrichlorosilane (DTS) to lower interfacial trap densities and improve device performance. In structures with a Ta$_2$O$_5$ gate dielectric, a thin buffer layer of SiO$_2$ (10 nm) is grown just below the polymer for deposition of DTS. Devices suitable for simultaneous electrical and spectroscopic

characterization contained source and drain electrodes, while structures optimized for IR measurements, in order to obtain the highest possible quality optical data, contained a single terminal enclosing a 3 mm$^2$ area (inset in Fig. 2). Previous microspectroscopy studies have determined that the charge injection landscape in polymer OFETs with low leakage SiO$_2$ gate insulator remains uniform over centimeter length scales.[16]

Current-voltage ($I$-$V$) characteristics of our OFETs with channel widths of 1 mm and channel lengths of 5 $\mu$m were obtained using a Keithley 4200 Semiconductor Parametric Analyzer and a Signotone Micromanipulator S-1160 probe station. Transient current measurements were performed by a Keithley 6487 picoammeter, using ac square wave pulses with a period of 10 s for both electron and hole injection.

Infrared transmission data were acquired in vacuum using a Bruker Vertex 70v FT-IR spectrometer with a spectral resolution of 8 cm$^{-1}$. Broadband light from a SiC thermal source was focused onto a liquid nitrogen-cooled HgCdTe (MCT) or InSb IR detector for mid-IR (750–6500 cm$^{-1}$) and near-IR (5000–10 000 cm$^{-1}$) measurements, respectively. Raman spectra were obtained by a Bruker Senterra dispersive Raman microscope using an excitation laser of wavelength 532 nm. All electrical and optical measurements were performed at room temperature.

In order to obtain frequency-dependent optical constants of the studied polymers we performed variable angle spec-troscopic ellipsometry (VASE) measurements on thin films spin-coated onto unpatterned substrates. Data were recorded using a commercial Woollam ellipsometer (IR-VASE) based on a Michelson interferometer (Bruker 66vs), covering the energy range 0.05–0.7 eV. The ellipsometric parameters $\Psi$ and $\Delta$ are related to the Fresnel reflection coefficients for $p$- and $s$- polarized light ($R_p$ and $R_s$) through the equation $\frac{R_p}{R_s} = \tan(\Psi)e^{i\Delta}$. The complex dielectric function of each polymer was modeled by considering a single Kramers-Kronig consistent Cody-Lorentz (C-L) oscillator[20] to fit the ellipsometric data. This model has been used to successfully describe optical absorption of a disordered semiconductor near the band edge.[21] Data for each polymer on SiO$_2$/Si at incidence angles of 60° and 75° were used for modeling.

## III. RESULTS

The bottom panels in Fig. 1 show typical output curves for OFETs based on small-gap polymers PBBTPD [Fig. 1(a)] and PBBTCD [Fig. 1(b)]. The observed transistor behavior is characteristic of ambipolar FET devices:[22,23] for small, negative gate voltage $V_{GS}$, holes are injected from the source electrode to form a relatively uniform charge distribution in the conduction channel. As the drain bias $V_{DS}$ is increased beyond $V_{GS}$, the hole density at the drain decreases to zero, and the drain potential with respect to the gate surpasses the threshold
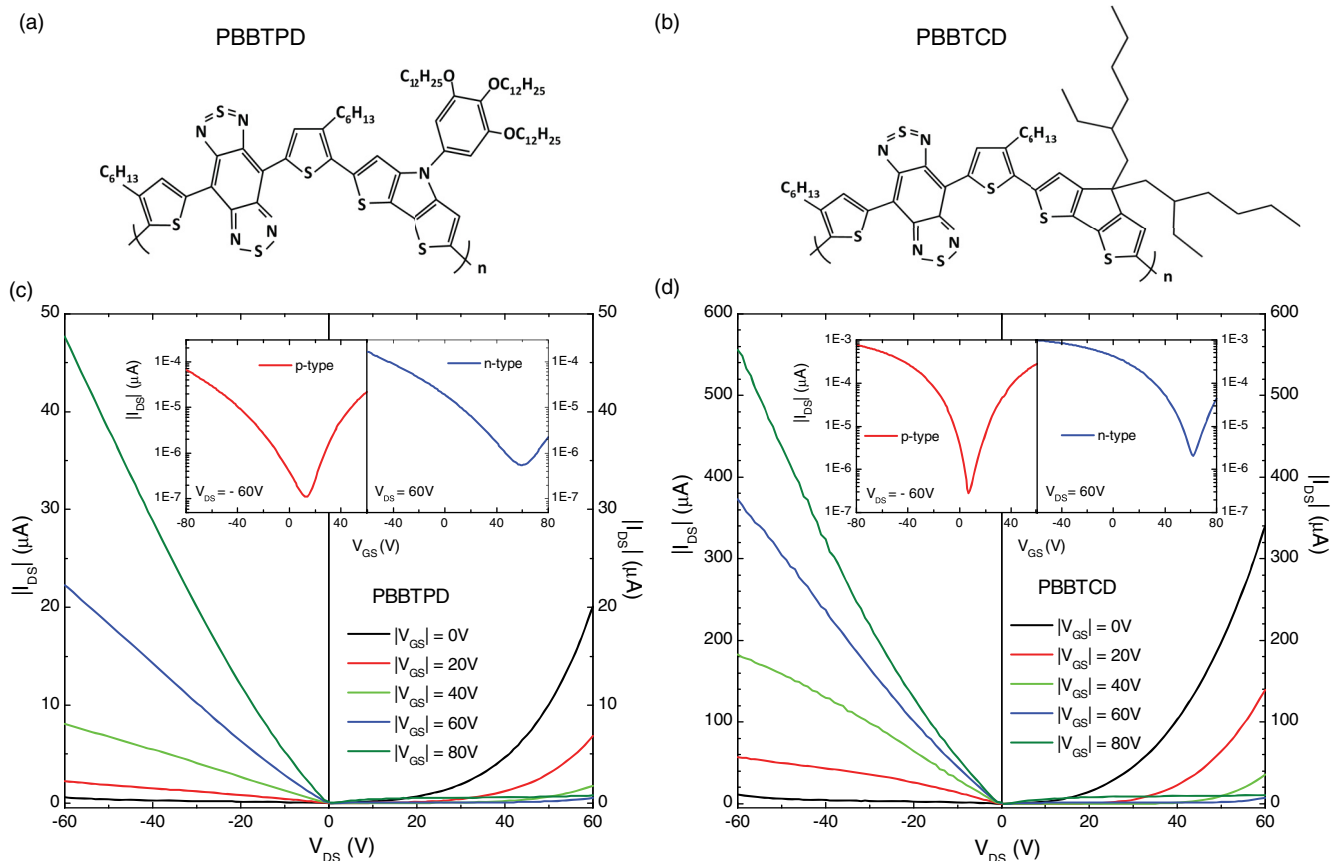


FIG. 1. (Color online) Top panels: Chemical structure of (a) PBBTPD and (b) PBBTCD. Bottom panels: $I$-$V$ output curves for a typical (c) PBBTPD- and (d) PBBTCD-based OFET with SiO$_2$ gate dielectric. Insets: OFET transfer characteristics using $|V_{DS}| = 60$ V for $p$-type (red curve) and $n$-type (blue curve) operation.

for electron injection ($V_{GD} > 0$ V neglecting trap states). Thus during ambipolar operation there exist spatially separated regions of accumulated electrons and holes occupying a common conduction channel in the polymer. The contribution of both types of charge carriers to the source-drain current ($I_{DS}$) results in diodelike behavior seen in the $I$-$V$ output characteristics. At high enough gate voltage, such that both $V_{GS}$ and $V_{GD}$ are of the same polarity, the channel is populated with only one type of charge carrier, and transport becomes unipolar. For this configuration, conventional FET behavior is recovered with $p$-type ($n$-type) operation for $V_{GS} < 0$ V ($V_{GS} > 0$ V), demonstrating saturation of the drain current at high $V_{DS}$. The "V" shape of the transfer curves [insets in Figs. 1(c) and 1(d)] is an additional hallmark of ambipolar charge injection, with the minimum signifying a transition from ambipolar to unipolar conduction.

Charge carrier mobilities were extracted using the conventional equation describing FET operation in the saturation regime:[24]

$$I_{DS} = \frac{1}{2}\frac{W}{L}\mu C_i(V_{GS} - V_T)^2, \qquad (1)$$

with mobility determined from $\partial|I_{GS}|^{1/2}/\partial V_{GS}$. Unipolar transport regimes were used for this calculation since during ambipolar operation it is difficult to distinguish the separate electron and hole contributions to the current. Average mobilities for electrons and holes, respectively, were $\mu_e = 8.2 \times 10^{-3}$ cm$^2$ V$^{-1}$ s$^{-1}$, $\mu_h = 9.6 \times 10^{-3}$ cm$^2$ V$^{-1}$ s$^{-1}$ for PBBTPD, and $\mu_e = 0.11$ cm$^2$ V$^{-1}$ s$^{-1}$, $\mu_h = 0.072$ cm$^2$ V$^{-1}$ s$^{-1}$ for PBBTCD, demonstrating ambipolar transport with similar $p$-type and $n$-type performance.[13] Due to the sensitivity of electronic transport to charge traps arising from film deposition and fabrication conditions, threshold voltages for electron injection tended to vary substantially among different devices.

We used infrared spectroscopy to probe the electronic excitations associated with injecting both electrons and holes into DA polymer films. The use of a rectangular electrode structure enclosing the illuminated area (inset in Fig. 2) ensures an electrostatic charge configuration, equivalent to grounding the source and drain electrodes, while maximizing the IR signal. Figure 2(a) shows IR transmission spectra $T(\omega, V_{GS})$ for a PBBTPD device plotted at various $V_{GS}$, normalized by $T(\omega, V_{GS} = 0$ V). Typically, differential spectra $\Delta T(\omega)/T(\omega)$ are better suited than absolute $T(\omega)$ measurements for studying charge- and field-induced changes in IR transmission, which are usually extremely small ($10^{-3}$–$10^{-4}$) and require very high accuracy. The red curves in Fig. 2 indicate $p$-type operation ($V_{GS} < 0$ V), while the blue curves indicate $n$-type operation ($V_{GS} > 0$ V). To facilitate the discussion, we denote three separate frequency regions in the spectra as regions A, B, and C, described in more detail below. Spectra are plotted in 10 V increments except for region A in Fig. 2(b) (5 V increments). Data in region A were obtained through transmission measurements for Ta$_2$O$_5$-based devices, while spectra in regions B and C were recorded for devices with a SiO$_2$ gate insulator. SiO$_2$/Si provides an ideal oxide/substrate interface with extremely low leakage currents and long-term device stability. However, excitations in the polymer below 1500 cm$^{-1}$ are obscured by Drude absorption in $n$-Si and
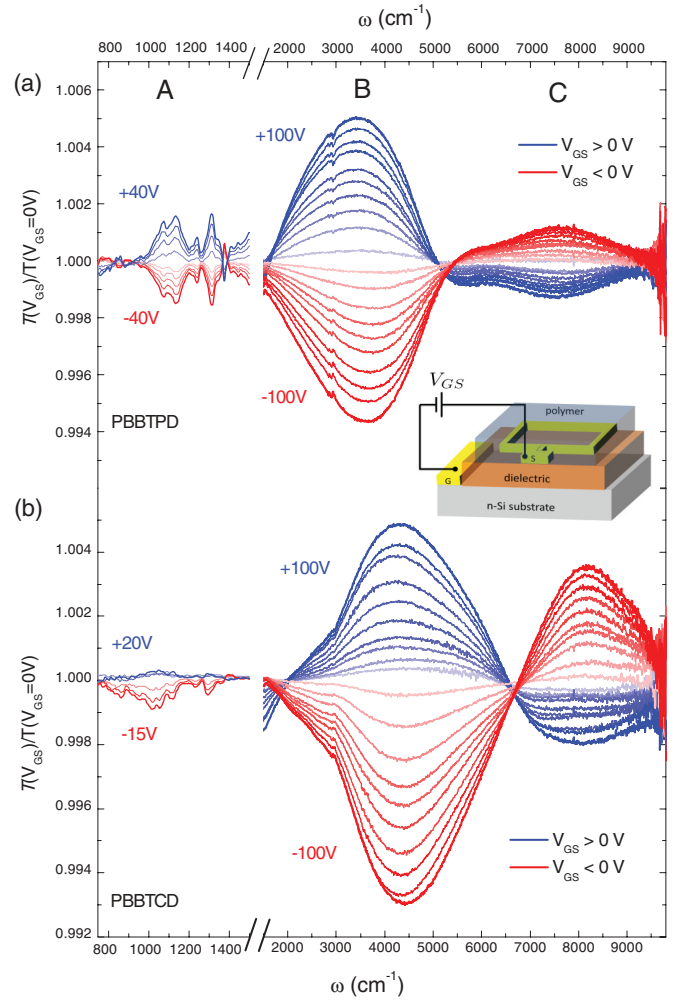


FIG. 2. (Color online) Voltage-induced change in transmission spectra $T(\omega, V_{GS})/T(\omega, V_{GS} = 0$ V) for structures employing (a) PBBTPD and (b) PBBTCD as the active semiconductor. Blue curves indicate $n$-type operation ($V_{GS} > 0$ V), that is, electron injection; red curves indicate $p$-type operation ($V_{GS} < 0$ V), that is, hole injection. Spectra from 750 to 1500 cm$^{-1}$ are representative data for devices with Ta$_2$O$_5$ gate insulator, where strong absorption due to the substrate is absent. Inset in (a) is the schematic of single-contact device architecture used for IR and capacitance measurements.

phonon modes in SiO$_2$. For devices based on Ta$_2$O$_5$, a high-$\kappa$ dielectric, in most cases no Drude absorption in the silicon is observed, and the oxide does not possess any IR-active phonons in the experimental range of interest.

We start with the features originating from hole injection [red curves in Fig. 2(a)] for negative gate voltage. In the range 750–1500 cm$^{-1}$, labeled as region A, several sharp absorption peaks (dips in transmission) are observed, a prominent absorption band centered at 3400 cm$^{-1}$ defines region B, while a broad increase in transmission from 5000 to 9000 cm$^{-1}$ is described as region C. The oscillator strength of all excitations systematically increases with the applied gate voltage.

The injection of electrons [blue curves in Fig. 2(a)] results in the appearance of features occurring at nearly the same frequencies compared to hole doping. Interestingly, however, the

change in oscillator strength for each excitation demonstrates the opposite dependence on the applied field: The absorptions in regions A and B are suppressed, while a new absorption appears in region C. Further increasing of the gate voltage to higher positive values leads to systematic suppression of the features in regions A and B, while strengthening the absorption in region C. All these effects mirror the evolution of the spectra with hole doping.

Figure 2(b) displays field-modulated transmission spectra for PBBTCD, a higher-mobility polymer of the same BBT-acceptor family. Similar IR features and field dependence compared to PBBTPD are observed. Notable differences, however, include a slightly different line shape and blueshift of the excitations in regions B and C. Additionally, the sharp resonances in region A occur at lower frequencies. Lastly, there is a more pronounced asymmetry in the strength of the modulation of the spectra, with positive gate-induced features being generally weaker than those for hole doping. The mirrorlike behavior reflected in the IR spectra for both polymers is highly reproducible, and was observed in over 30 structures, consisting of both two- and three-terminal devices. The symmetry in the intensity of the positive and negative voltage-induced features is more common in PBBTPD devices, while the spectra tend to be more asymmetric in most PBBTCD structures. Later we discuss a possible connection of these differences to transport in the two polymers.

In order to explain the voltage dependence of the IR transmission spectra, it is important to understand the behavior of absolute absorption in the polymer films. We employed spectroscopic ellipsometry to obtain a detailed characterization of the absorption edge for both polymers, which occurs in the vicinity of the gate-induced features. Due to the limited device area, as well as other constraints imposed by field-effect devices (e.g., electrodes), ellipsometry was performed on thicker polymer films deposited on unpatterned silicon substrates. Figure 3 shows the absorption coefficient as a function of frequency $\alpha(\omega)$ determined from analysis of the ellipsometric data as described in Sec. II. The complex refractive index $N = n + ik$ was extracted from a Cody-Lorentz oscillator model, where $\alpha(\omega)$ was obtained via $k = \alpha c/\omega$. The optical band gap $E_g$ was extracted by extrapolating the linear portion of the absorption edge to the horizontal axis (red and blue dotted lines). The values of $E_g$ obtained were 4113 cm$^{-1}$ (0.51 eV) for PBBTPD and 4758 cm$^{-1}$ (0.59 eV) for PBBTCD, which are very close to those observed in absorbance spectra.[13] Experimental and model ellipsometry data for PBBTPD on SiO$_2$/Si obtained at an incidence angle of 60° are shown in the inset of Fig. 3.

In addition to an ellipsometric analysis of the absorption edge, we carried out Raman spectroscopy measurements to assist in the examination of the sharp doping-induced peaks in region A of Fig. 2. The bottom panel of Fig. 4 shows Raman spectra for thin films of PBBTPD (violet line) and PBBTCD (green line) on SiO$_2$/Si, while the top panel reproduces data from Fig. 2. Though spectra for both polymers show a similar pattern, Raman modes for PBBTCD are distinct from those of PBBTPD. Important to note is the large discrepancy in energies associated with the voltage-induced peaks in PBBTPD compared to PBBTCD, in contrast with the rather small variations in the Raman modes between the two polymers.
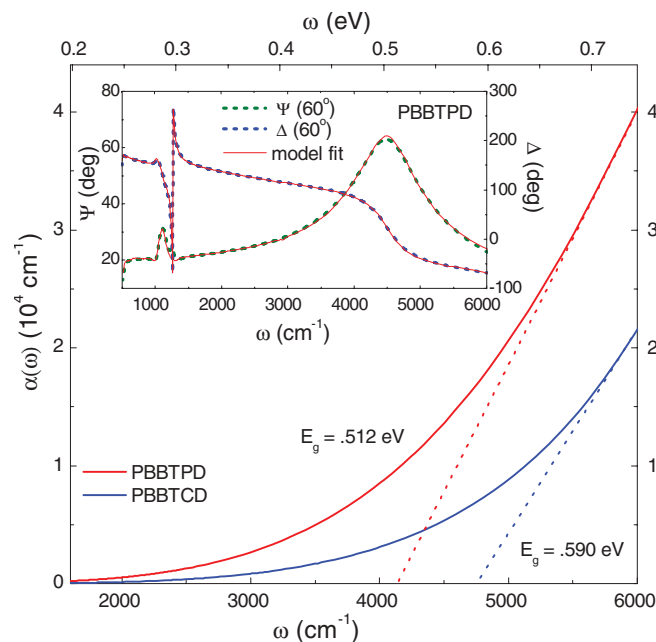


FIG. 3. (Color online) Absorption coefficient $\alpha(\omega)$ for PBBTPD (red solid line) and PBBTCD (blue solid line) thin films, obtained from modeling of ellipsometric data. Dotted lines indicate linear extrapolation of absorption edge to determine the energy band gap $E_g$ for each polymer. Inset: Experimental ellipsometry data $\Psi$ (green dashed line) and $\Delta$ (blue dashed line) for PBBTPD on SiO$_2$/Si. Spectra were acquired at an incidence angle of 60° and are plotted with corresponding model fits (red solid lines).
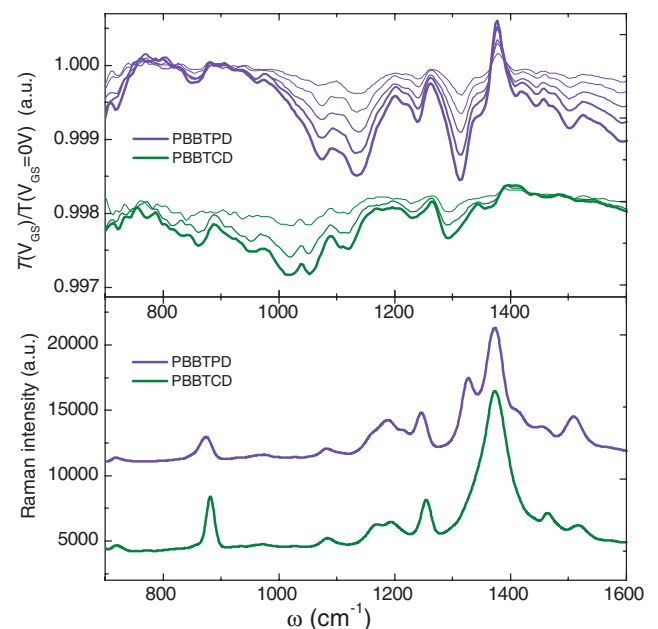


FIG. 4. (Color online) Top panel: Voltage-induced peaks for PBBTPD (violet curves) and PBBTCD (green curves) reproduced from Fig. 2. Bottom panel: Raman spectra for PBBTPD (violet line) and PBBTCD (green line) thin films on SiO$_2$/Si.

In general, the optical functions of a material can yield important information about physical processes governing the dynamics of electrons and holes through the frequency sum rule $\int_0^\infty \frac{nc}{4\pi}\alpha(\omega)d\omega \propto \frac{N_e}{m_{\text{eff}}}$. This expression connects the density of charges $N_e$ (with effective mass $m_{\text{eff}}$) contributing to the electromagnetic response, to the integral of the absorption coefficient over all frequencies.[25] In the spirit of this generic sum rule result, we define a quantity $\Delta I$ that relates the injected charge carriers to the field-induced change in IR transmission as

$$\Delta I = \int_{1400}^{5200} \frac{T(\omega, V_{\text{GS}})}{T(\omega, V_{\text{GS}} = 0\,\text{V})} d\omega, \qquad (2)$$

where the limits of integration were chosen over the feature in region B near the onset of the absorption edge. Plotted on the left axis of Fig. 5(a) is $|\Delta I|$ as a function of $V_{\text{GS}}$ (red squares). $\Delta I$ very clearly evolves linearly with the applied electric field for both electron and hole injection.

For structures with a $SiO_2$ gate insulator, it is safe to model device behavior as an ideal parallel plate capacitor, where the induced charge density increases linearly with the applied electric field.[16] We independently verified this assumption by acquiring transient current data $I_{\text{GS}}(t)$ for a PBBTPD-based device [Fig. 5(b)], where $|V_{\text{GS}}|$ is applied

as square wave pulses with a period of $T = 10$ s. The charging currents measured during the first few seconds of each pulse can be integrated to yield the total number of injected charges $Q = \int [I_{\text{GS}}(t) - I_L] dt$, and thus the two-dimensional (2D) carrier density $n_{2D} = Q/A$, where $I_L$ is the leakage current and the active device area is $A = 1$ cm$^2$. $n_{2D}$ as a function of $V_{\text{GS}}$ is plotted on the right axis of Fig. 5(a) (black squares). Establishing the linear relationship between the applied electric field $V_{\text{GS}}$ (i.e., injected charge carrier density) and the field-induced change in IR transmission $\Delta I$ is important for interpretations presented in the next section. The obtained values for $n_{2D}$ are in good agreement with the maximum carrier densities typically achieved in OFETs employing oxide gate insulators.[16]

## IV. DISCUSSION

The salient characteristic of pristine BBT-based copolymers is the exceptionally narrow energy band gaps observed in absorbance measurements[13,14] and confirmed through our ellipsometric data plotted in Fig. 3. Gap values extracted from these data, 0.51 eV for PBBTPD and 0.59 eV for PBBTCD, are among the smallest for ambipolar DA conjugated polymers. Additionally, there is considerable broadening of the absorption edge, which is expected for a disordered, amorphous polymer thin film. The energy range associated with the disorder-induced band tail states, and of the interband transitions in general, is relevant to the observed gate-induced transformations of the spectra.

There are multiple processes that give rise to the features we observe in the IR transmission data in Fig. 2. We start this analysis with a discussion of the resonances in region A. The addition of charge carriers to a neutral polymer commonly leads to the formation of infrared-active vibrational modes (IRAVs): Distortions in the polymer backbone due to injected charges.[26] The excess charge couples to symmetric Raman modes, inducing a transition dipole moment that renders these modes IR active. The manner in which sharp peaks induced by hole injection in region A of Fig. 2 intensify systematically with increasing gate voltage is consistent with previous spectroscopic studies of conjugated polymer OFETs.[16] Observation of a distinct IRAV spectrum each for PBBTPD and PBBTCD is a natural consequence of the different chemical structure, also reflected in the Raman data shown in Fig. 4. The lower frequencies associated with IRAVs in PBBTCD, indicative of weaker localization of charge carriers, is discussed later.

The systematic increase in transmission of IRAV features for positive gate voltages remains curious. The amplitude mode (AM) formalism[26,27] and subsequent theoretical efforts,[28–31] aimed at providing a model for IRAV bands in polymers, do not discriminate between the electrons and holes. However, studies investigating electrochemical $n$ and $p$ doping of the same polythiophene hosts reveal distinct IRAV modes induced for positive and negative charge carriers.[32] Thus, one would expect to observe a different series of absorption peaks for electron injection, as opposed to suppression of the same absorption features. The observed behavior is consistent with the assumption that IRAV absorption persists in the ungated polymer as will be detailed below.



FIG. 5. (Color online) (a) Left axis: Field-induced change in transmission $|\Delta T|$ (red triangles) integrated from 1400 to 5200 cm$^{-1}$ and plotted as a function of $V_{\text{GS}}$. Right axis: 2D density of induced electrons or holes $n_{2D}$ (black triangles) as a function of $V_{\text{GS}}$. $n_{2D}$ was obtained by integrating the transient current $I_G$ in (b), after subtracting leakage, and assuming an accumulation layer thickness of $d = 2$ nm and an active area of $A = 0.5$ cm$^2$. (b) $I_G(t)$ data for a PBBTPD thin-film device, applying $|V_{\text{GS}}| = 10$ (light gray), 50 (dark gray), and 100 V (black) as a pulse waveform with period $T = 10$ s.

The assignment of the broad mid- and near-IR features (regions B and C) is less straightforward. Typically, concomitant with IRAVs are large absorption bands signifying optical transitions to midgap localized states, observed in many previous spectroscopic studies of conducting polymers.[33–39] Formation of these localized states is related to geometrical relaxation (lattice distortion) in nondegenerate ground state polymers due to excess charges, usually described as polarons or bipolarons. In addition to unique IRAVs, a distinct polaron feature is expected to arise each from electron and hole injection, confirmed through chemical doping studies in Ref. [32]. Recent data on polyselenophene-based ambipolar OFETs from Chen *et al.* also reveal spectroscopic evidence of electron and hole polaron absorption, in response to an applied gate bias.[40] The intensity of these excitations increases at the expense of the (bleached) neutral absorption. In other intrinsically ambipolar systems, such as monolayer and bilayer graphene, either polarity of gate voltage results in increased absorption at far- and mid-IR frequencies.[41–45] This expected behavior of both electron and hole-induced absorption stands in contrast with what we observe in our data. The mirror-symmetric form of the spectra in Fig. 2 is more in line with what has been seen recently in heavily doped semiconductors.[46]

It is possible that these IRAV and broad excitations persist even in the ungated film due to an intrinsic charge-transfer mechanism during polymerization, or alternatively due to unintentional doping from extrinsic factors such as oxidation or trapping.[47] If there is an already present hole-induced polaron band, the act of injecting electrons by gating reduces the number of positively charged polymer segments, thereby suppressing the intensity of this broad absorption feature. The pronounced symmetry of the IR data for gated structures, with respect to the polarity of $V_{GS}$, would thus be the result of increasing or decreasing the oscillator strength of extrinsic hole-induced absorptions. In a similar vein, the behavior of the spectra in region C could reflect bleaching/restoration of the neutral absorption as holes or electrons are injected, respectively. In essence, the primary consequence of injection of electrons in the mid-IR spectra is to compensate for holes that are already present in our polymers. Based on the symmetry reflected in the data, the charge neutrality point is never reached within the range of $V_{GS}$ we apply. Additionally, an initial population of excess holes implies the existence of IRAVs without an applied field. However, IRAV modes could not be definitively distinguished from intrinsic IR vibrational absorptions in absolute transmission measurements of the polymer film.

The presence of mobile holes in the ungated film has implications for the prospect of ambipolar device operation. Electron transport is especially sensitive to the presence of trap states, and such charged defects would assuredly compromise device performance by capturing mobile electrons. The consistency of the symmetric behavior in the IR transmission data presents an interesting conundrum to the origin of the intrinsic ambipolarity in BBT-based copolymers. Though electron transport varied greatly across structures with source and drain electrodes (for which OFET *I-V* characteristics could be measured), both ambipolar transport and symmetric IR spectra have been observed for at least a few devices. This would seem to rule out the possibility of degradation before every spectroscopic measurement, due to ambient air exposure. The simplest physical picture of enhancement/suppression of hole-polaron and IRAV absorption, seemingly evident from the IR spectra, implies that movement of the Fermi level in response to charge injection takes place entirely within a polaron band in the vicinity of the HOMO band edge. The possibility of such a system sustaining electron transport with mobility comparable to holes is dubious at best, calling for perhaps more complicated interpretations of the electronic structure of these particular DA materials.

In light of the observation of IR features associated with localized states, as well as transport data demonstrating relatively high carrier mobility, we posit the prospect of phase separation and coexistence in the copolymer. Many theoretical models of conducting polymers involve a continuous electronic transition from localized to itinerant charge carrier motion with doping, as trap states are eventually filled up to the "mobility edge."[48] An underlying assumption is that of a homogeneous film, a questionable postulate. Perhaps a more realistic picture of electronic transport in disordered polymer films is the one allowing for coexisting regions dominated by either localized or delocalized ("metallic") transport. Indeed phase coexistence of both localized and delocalized states has been observed in highly doped polyacetylene,[35] polyaniline,[49,50] and P3HT.[51,52] Our spectroscopic probe interrogates the higher energy bound states characteristic of localized charges, while OFET transport data are dominated by mobile carriers.

The response of delocalized carriers to light excitation typically manifests in increased far-IR Drude-like absorption.[17,25,35,49–52] In polyaniline, a significant metallic optical response was observed concurrent with IRAV modes, and was modeled as a conductor with molecular scale disorder and mesoscale inhomogeneity associated with phase separation.[49] Such a Drude-like response in the DA polymers investigated here would likely be masked by the overwhelmingly strong free-carrier absorption in the *n*-doped silicon substrate. Also consistent with the notion of coexisting localized and itinerant carriers is the weaker suppression of absorptions in PBBTCD devices for electron injection. IRAVs in PBBTCD have smaller energies and are generally less intense compared to PBBTPD, reflecting a smaller degree of localization, consistent with transport measurements that show an order of magnitude higher electron and hole mobility. Detailed studies of doping-induced vibrational modes in conducting polymers show that the degree to which IRAV frequencies are redshifted from the symmetric Raman modes is related to a "pinning parameter" that characterizes the localization of the injected charge carriers.[53–55] Theoretically, a lower vibrational frequency (i.e., smaller force constant) reflects smaller electron-phonon coupling, leading to improved charge transport. Additionally, if suppression of the polaron absorption in region B is associated with trapped electrons, the symmetry in the IR data is an indicator of compensation by holes. Thus the weaker suppression of hole-induced absorptions for positive gate voltages in PBBTCD suggests an increase in the population of mobile carriers, leading to better electron transport.

Lastly, we comment on the possible role of field-induced modification of the band edge states (electroabsorption), that is, the Stark effect. The observed effects in regions B and C of Fig. 2 clearly occur in the vicinity of the broadened band edge.

The apparent blueshift of this structure for PBBTCD, which possesses a slightly larger band gap than PBBTPD, further strengthens the connection between these features and the polymer absorption edge. Electroabsorption (EA) spectra of conjugated polymers are usually interpreted in terms of either the linear or quadratic Stark effect.[56–66] The latter originates from induced dipoles, as the applied electric field mixes the low energy states of odd parity with the excited state continuum at higher energies.[58] The energy shift associated with a quadratic Stark shift is independent on the sign of the applied field, which is inconsistent with the linear behavior we observe in Fig. 5(a). The linear Stark effect, which is due to permanent dipoles, can explain the symmetric form of the broad absorptions, provided there is a large intrinsic built-in electrical dipole moment, as well as interfacial ordering at the semiconductor/insulator interface.[67] The origin of such a dipole, as well as a mechanism by which ordering near the interface could occur, is unclear. We carried out density-functional theory (DFT) calculations for isolated donor-acceptor molecules using the Octopus code[68] with PBE[69,70] functionals, and we do find a significant ground state dipole moment for both PBBTPD (3.47 D) and PBBTCD (1.31 D), as well as a strengthening of the dipole in the dimers.[71] However, compared to the more plausible picture of polaron absorption, and the failure of the linear Stark effect to explain the behavior of IRAVs, we feel that any electroabsorptive effects are most likely minor and/or unnoticeable.

## V. SUMMARY

We have systematically investigated the infrared response of charge injection in ambipolar OFETs based on narrow-gap DA polymers PBBTPD and PBBTCD. In both polymers, hole doping produces several sharp absorption peaks in the range 800–1400 cm$^{-1}$ associated with injected charges and identified as IRAVs. Additionally, hole injection results in the appearance of a broad absorption near the band edge in both PBBTPD and PBBTCD, followed by an increase in transmission above the energy gap. For positive gate voltages, the intensity of charged excitations occurring at the same frequencies weakens with increasing field, leading to a mirrorlike behavior in the IR spectra (i.e., hole-induced absorptions are suppressed). An observed blueshift of field-induced IR features in PBBTCD is consistent with the slightly larger energy band gap, and suggests the origin of the broad structures to be closely linked to the absorption edge of the HOMO-LUMO transition.

The symmetry of the IR transmission data with respect to the polarity of the gate voltage presents a challenge to understanding the electronic excitations associated with ambipolar charge injection in narrow-gap polymers. The totality of our data indicates a significant self-doping of holes that is modified by charge injection. Clear observations of both hole and electron transport with high carrier mobility strongly suggest an inhomogeneous, phase-separated conducting polymer. A high-resolution real space probe is necessary to resolve such inhomogeneities, and explore the molecular effects of electron and hole injection on the electronic structure of BBT-based DA copolymers.

*okhatib@physics.ucsd.edu

[1] T. W. Kelley, P. F. Baude, C. Gerlach, D. E. Ender, D. Muyres, M. A. Haase, D. E. Vogel, and S. D. Theiss, Chem. Mater. **16**, 4413 (2004).

[2] H. E. Katz and J. Huang, Annu. Rev. Mater. Res. **39**, 71 (2009).

[3] S. Wang, M. Kappl, I. Liebewirth, M. Müller, K. Kirchhoff, W. Pisula, and K. Müllen, Adv. Mater. **24**, 417 (2012).

[4] H. Klauk, Chem. Soc. Rev. **39**, 2643 (2010).

[5] E. J. Meijer, D. M. De Leeuw, S. Setayesh, E. Van Veenendaal, B.-H. Huisman, P. W. M. Blom, J. C. Hummelen, U. Scherf, and T. M. Klapwijk, Nat. Mater. **2**, 678 (2003).

[6] Z. Chen, M. J. Lee, R. S. Ashraf, Y. Gu, S. Albert-Seifried, M. M. Nielson, B. Schroeder, T. D. Anthopoulos, M. Heeney, I. McCulloch, and H. Sirringhaus, Adv. Mater. **24**, 647 (2012).

[7] S. Cho, J. Lee, M. Tong, J. H. Seo, and C. Yang, Adv. Funct. Mater. **21**, 1910 (2011).

[8] T. T. Steckler, X. Zhang, J. Hwang, R. Honeyager, S. Ohira, X.-H. Zhang, A. Grant, S. Ellinger, S. A. Odom, D. Sweat, D. B. Tanner, A. G. Rinzler, S. Barlow, J.-L. Brédas, B. Kippelen, S. R. Marder, and J. R. Reynolds, J. Am. Chem. Soc. **131**, 2824 (2009).

[9] C. J. DuBois, K. A. Abboud, and J. R. Reynolds, J. Phys. Chem. B **108**, 8550 (2004).

[10] J.-L. Brédas, J. Chem. Phys. **82**, 3808 (1985).

[11] J.-L. Brédas, A. J. Heeger, and F. Wudl, J. Chem. Phys. **85**, 4673 (1986).

[12] E. Ahmed, S. Subramaniyan, F. S. Kim, H. Xin, and S. A. Jenekhe, Macromolecules **44**, 7207 (2011).

[13] J. D. Yuen, R. Kumar, D. Zakhidov, J. Seifter, B. Lim, A. J. Heeger, and F. Wudl, Adv. Mater. **23**, 3780 (2011).

[14] X. Zhang, T. T. Steckler, R. R. Dasari, S. Ohira, W. J. Potscavage, Jr, S. P. Tiwari, S. Coppée, S. Ellinger, S. Barlow, J.-L. Brédas, B. Kippelen, J. R. Reynolds, and S. R. Marder, J. Mater. Chem. **20**, 123 (2009).

[15] J. D. Yuen, M. Wang, J. Fan, D. Sheberla, M. Kemei, M. Scarongella, S. Valouch, T. Pho, E. C. Chestnut, N. Banerji, M. Bendikov, and F. Wudl (unpublished).

[16] Z. Q. Li, G. M. Wang, N. Sai, D. Moses, M. C. Martin, M. DiVentra, A. J. Heeger, and D. N. Basov, Nano Lett. **6**, 224 (2006).

[17] M. Fischer, M. Dressel, B. Gompf, A. K. Tripathi, and J. Pflaum, Appl. Phys. Lett. **89**, 182103 (2006).

[18] T. Mills, L. G. Kaake, and X.-Y. Zhu, Appl. Phys. A **95**, 291 (2009).

[19] H. Matsui and T. Hasegawa, Appl. Phys. Lett. **95**, 223301 (2009).

[20] A. S. Ferlauto, G. M. Ferreira, J. M. Pearce, C. R. Wronski, R. W. Collins, X. Deng, and G. Ganguly, J. Appl. Phys. **92**, 2424 (2002).

[21]P. J. van den Oever, M. C. M. van de Sanden, and W. M. M. Kessels, J. Appl. Phys. **101**, 123529 (2007).

[22]E. C. P. Smits, T. D. Anthopoulos, S. Setayesh, E. van Veenendaal, R. Coehoorn, P. W. M. Blom, B. de Boer, and D. M. de Leeuw, Phys. Rev. B **73**, 205316 (2006).

[23]J. Zaumseil and H. Sirringhaus, Chem. Rev. **107**, 1296 (2007).

[24]D. Braga and G. Horowitz, Adv. Mat. **21**, 1473 (2009).

[25]F. Wooten, *Optical Properties of Solids* (Academic, New York, 1972).

[26]B. Horovitz, Solid State Commun. **41**, 729 (1982).

[27]E. Ehrenfreund, Z. Vardeny, O. Brafman, and B. Horovitz, Phys. Rev. B **36**, 1535 (1987).

[28]M. Del Zoppo, C. Castiglioni, P. Zuliani, and G. Zerbi, in *Handbook of Conducting Polymers*, 2nd ed., edited by T. A. Skotheim, R. L. Elsenbaumer, and J. R. Reynolds (Marcel Dekker, New York, 1988), Chap. 28.

[29]G. Zerbi, M. Gussoni, C. Castiglioni, in *Conjugated Polymers*, edited by J. L. Brédas and R. Silbey (Kluwer Academic, Dordrecht, 1991), p. 435.

[30]E. A. Ehrenfreund and Z. V. Vardeny, Proc. SPIE **3145**, 324 (1997).

[31]A. Girlando, A. Painelli, and Z. G. Soos, J. Chem. Phys. **98**, 7459 (1993).

[32]H. Neugebauer, J. Electroanal. Chem. **563**, 153 (2004).

[33]Y. H. Kim, D. Spiegel, S. Hotta, and A. J. Heeger, Phys. Rev. B **38**, 5490 (1988).

[34]A. J. Heeger, S. Kivelson, J. R. Schrieffer, and W.-P. Su, Rev. Mod. Phys. **60**, 781 (1988).

[35]Y. H. Kim and A. J. Heeger, Phys. Rev. B **40**, 8393 (1989).

[36]R. Österbacka, C. P. An, X. M. Jiang, and Z. V. Vardeny, Science **287**, 839 (2000).

[37]X. M. Jiang, R. Österbacka, O. Korovyanko, C. P. An, B. Horovitz, R. A. J. Janssen, and Z. V. Vardeny, Adv. Funct. Mater. **12**, 587 (2002).

[38]R. Österbacka, X. M. Jiang, C. P. An, B. Horovitz, and Z. V. Vardeny, Phys. Rev. Lett. **88**, 226401 (2002).

[39]B. Horovitz, R. Österbacka, and Z. V. Vardeny, Synth. Met. **141**, 179 (2004).

[40]Z. Chen, M. Bird, V. Lemaur, G. Radtke, J. Cornil, M. Heeney, I. McCulloch, and H. Sirringhaus, Phys. Rev. B **84**, 115211 (2011).

[41]Z. Q. Li, E. A. Henriksen, Z. Jiang, Z. Hao, M. C. Martin, P. Kim, H. L. Stormer, and D. N. Basov, Nat. Phys. **4**, 532 (2008).

[42]L. M. Zhang, Z. Q. Li, D. N. Basov, M. M. Fogler, Z. Hao, and M. C. Martin, Phys. Rev. B **78**, 235408 (2008).

[43]Z. Q. Li, E. A. Henriksen, Z. Jiang, Z. Hao, M. C. Martin, P. Kim, H. L. Stormer, and D. N. Basov, Phys. Rev. Lett. **102**, 037403 (2009).

[44]Y. Zhang, T.-T. Tang, C. Girit, Z. Hao, M. C. Martin, A. Zettl, M. F. Crommie, Y. R. Shen, and F. Wang, Nature (London) **459**, 820 (2009).

[45]J. Horng, C.-F. Chen, B. Geng, C. Girit, Y. Zhang, Z. Hao, H. A. Bechtel, M. Martin, A. Zettl, M. F. Crommie, Y. R. Shen, and F. Wang, Phys. Rev. B **83**, 165113 (2011).

[46]B. C. Chapler, S. Mack, L. Ju, T. W. Elson, B. W. Boudouris, E. Namdas, J. D. Yuen, A. J. Heeger, N. Samarth, M. Di Ventra, R. A. Segalman, D. D. Awschalom, F. Wang, and D. N. Basov, Phys. Rev. B **86**, 165302 (2012).

[47]H. Sirringhaus, Adv. Mater. **21**, 3859 (2009).

[48]A. Salleo, T. W. Chen, A. R. Volkel, Y. Wu, P. Liu, B. S. Ong, and R. A. Street, Phys. Rev. B **70**, 115311 (2004).

[49]K. Lee, A. J. Heeger, and Y. Cao, Phys. Rev. B **48**, 14884 (1993).

[50]K. Lee, S. Cho, S. H. Park, A. J. Heeger, C.-W. Lee, and S.-H. Lee, Nature (London) **441**, 65 (2006).

[51]A. S. Dhoot, G. M. Wang, D. Moses, and A. J. Heeger, Phys. Rev. Lett. **96**, 246403 (2006).

[52]O. Khatib, B. Lee, J. D. Yuen, Z. Q. Li, M. Di Ventra, A. J. Heeger, V. Podzorov, and D. N. Basov, J. Appl. Phys. **107**, 123702 (2010).

[53]A. Cravino, H. Neugebauer, S. Luzzati, M. Catellani, A. Petr, L. Dunsch, and N. S. Sariciftci, J. Phys. Chem. B **106**, 3583 (2002).

[54]H. Neugebauer, C. Kvarnström, A. Cravino, T. Yohannes, and N. S. Sariciftci, Synth. Met. **116**, 115 (2001).

[55]M. Gussoni, C. Castiglioni, and G. Zerbi, in *Spectroscopy of Advanced Materials*, edited by R. J. H. Clark and R. E. Hester (Wiley, New York, 1991), p. 251.

[56]S. D. Phillips, R. Worland, G. Yu, T. Hagler, R. Freedman, Y. Cao, V. Yoon, J. Chiang, W. C. Walker, and A. J. Heeger, Phys. Rev. B **40**, 9751 (1989).

[57]G. Weiser, Phys. Status Solidi A **18**, 347 (1973).

[58]A. Horvath, G. Weiser, G. L. Baker, and S. Etemad, Phys. Rev. B **51**, 2751 (1995).

[59]L. Sebastian and G. Weiser, Chem. Phys. **62**, 447 (1981).

[60]I. H. Campbell, T. W. Hagler, D. L. Smith, and J. P. Ferraris, Phys. Rev. Lett. **76**, 1900 (1996).

[61]G. Weiser, Phys. Rev. B **45**, 14076 (1992).

[62]D. Guo, S. Mazumdar, S. N. Dixit, F. Kajzar, F. Jarka, Y. Kawabe, and N. Peyghambarian, Phys. Rev. B **48**, 1433 (1993).

[63]S. Al Jalali and G. Weiser, J. Non-Cryst. Solids **41**, 1 (1980).

[64]G. Weiser, J. Appl. Phys **43**, 5028 (1972).

[65]F. Feller and A. P. Monkman, Phys. Rev. B **60**, 8111 (1999).

[66]S. Haas, H. Matsui, and T. Hasegawa, Phys. Rev. B **82**, 161301 (2010).

[67]G. Horowitz, J. Mater. Res. **19**, 1946 (2004).

[68]A. Castro, H. Appel, M. Oliveira, C. A. Rozzi, X. Andrade, F. Lorenzen, M. A. L. Marques, E. K. U. Gross, and A. Rubio, Phys. Status Solidi B **243**, 2465 (2006).

[69]J. P. Perdew, K. Burke, and M. Ernzerhof, Phys. Rev. Lett. **77**, 3865 (1996).

[70]J. P. Perdew, K. Burke, and M. Ernzerhof, Phys. Rev. Lett. **78**, 1396(E) (1997).

[71]J. Wilson and M. Di Ventra (unpublished).